Received: 9 January 2020 | Revised: 16 April 2020 | Accepted: 17 April 2020

DOI: 10.1096/fj.202000073RRRRR

RESEARCH ARTICLE

THE FASEB JOURNAL

H19/TET1 axis promotes TGF-β signaling linked to endothelial-to-mesenchymal transition

Tiefeng Cao[1,2] | Ying Jiang[1,3] | Da Li[1,4] | Xiaoli Sun[1,5] | Yuanyuan Zhang[1,6] | Lingfeng Qin[7] | George Tellides[7] | Hugh S. Taylor[1] | Yingqun Huang[1]

[1]Department of Obstetrics, Gynecology, & Reproductive Sciences, Yale University School of Medicine, New Haven, CT, USA

[2]Department of Gynecology and Obstetrics, First Affiliated Hospital of Sun Yat-Sen University, Guangzhou, China

[3]Department of Obstetrics, Women's Hospital, Zhejiang University School of Medicine, Hangzhou, China

[4]Department of Obstetrics and Gynecology, Center of Reproductive Medicine, Shengjing Hospital of China Medical University, Shenyang, China

[5]Department of Obstetrics and Gynecology, Center of Reproductive Medicine, Affiliated Hospital of Nantong University, Nantong, China

[6]Department of Obstetrics and Gynecology, The First Affiliated Hospital of Nanjing Medical University, Nanjing, China

[7]Department of Surgery, Yale University School of Medicine, New Haven, CT, USA

Correspondence
Yingqun Huang, Department of Obstetrics, Gynecology, & Reproductive Sciences, Yale University School of Medicine, New Haven, CT 06510, USA.
Email: Yingqun.huang@yale.edu

Funding information
National Institute of Diabetes and Digestive and Kidney Diseases (NIDDK)

Abstract

While emerging evidence suggests the link between endothelial activation of TGF-β signaling, induction of endothelial-to-mesenchymal transition (EndMT), and cardiovascular disease (CVD), the molecular underpinning of this connection remains enigmatic. Here, we report aberrant expression of H19 lncRNA and TET1 in endothelial cells (ECs) of human atherosclerotic coronary arteries. Using primary human umbilical vein endothelial cells (HUVECs) and aortic endothelial cells (HAoECs) we show that TNF-α, a known risk factor for endothelial dysfunction and CVD, induces H19 expression which in turn activates TGF-β signaling and EndMT via a TET1-dependent epigenetic mechanism. We also show that H19 regulates TET1 expression at the posttranscriptional level. Further, we provide evidence that this H19/TET1-mediated regulation of TGF-β signaling and EndMT occurs in mouse pulmonary microvascular ECs in vivo under hyperglycemic conditions. We propose that endothelial activation of the H19/TET1 axis may play an important role in EndMT and perhaps CVD.

KEYWORDS

atherosclerosis, cardiovascular, EndMT, epigenetic, LncRNA

Abbreviations: CVD, cardiovascular disease; ECM, extracellular matrix; ECs, endothelial cells; EMT, epithelial-to-mesenchymal transition; EndMT, endothelial-to-mesenchymal transition; HAoECs, human aortic endothelial cells; Hcy, homocysteine; LncRNA, long noncoding RNA; SMCs, smooth muscle cells.

Tiefeng Cao, Ying Jiang, and Da Li contributed equally to this work.

1 | INTRODUCTION

Emerging evidence suggests that the evolutionarily conserved, developmentally regulated H19 long noncoding RNA (lncRNA) plays an important role in the pathogenesis of cardiovascular disease (CVD). Epidemiological studies have documented an association between common polymorphisms of H19 and the risk and severity of coronary artery disease and between increased plasma levels of H19 RNA and increased risks of coronary artery disease and heart failure.[1,2] H19 is prominently expressed in endothelial cells (ECs) and smooth muscle cells (SMCs) of prenatal rabbit aorta but becomes barely detectable in adult animals.[3] However, H19 is reexpressed in rat intima after blood vessel injury,[4] in left ventricle interstitial vascular structures of heart failure human patients,[5] and in human atherosclerotic plaques.[3] While H19 expression decreases in ECs of aging mice,[6] increased H19 expression in SMCs induces aortic aneurysm in animal models.[7,8] In an ApoE knockout (KO) atherosclerosis mouse model, upregulation of H19 expression was observed in aortic tissues (likely in both ECs and SMCs) and silencing H19 using antisense oligonucleotides attenuated disease progression.[9] Collectively, these findings suggest a causal role of H19 expression in ECs/SMCs in the pathogenesis of CVD.

The TET proteins (TET1, TET2, and TET3) are a recently discovered family of DNA demethylases that oxidize 5-methylcytosine (5mC) to 5-hydroxymethylcytosine (5hmC), which is subsequently converted to unmethylated cytosine by thymine DNA glycosylase coupled with base excision repair.[10] The process is highly dynamic and tightly regulated in a cell/tissue and developmentally dependent manner. While TET2 is enriched in mature contractile SMCs in normal vasculatures and its expression decreases in atherosclerotic lesions,[11-13] TET1 expression increases in atherosclerotic plaques.[14] As both H19 and TET2/TET1 are implicated in CVD, they may be mechanistically linked.

Endothelial-to-mesenchymal transition (EndMT) occurs during normal development and also contributes to the pathogenesis of CVD (reviewed in 15,16) including atherosclerosis,[17-19] myocardial infarction,[20] vascular malformation,[21] pulmonary hypertension,[22] portal hypertension,[23] vascular graft failure,[24,25] and cardiac fibrosis.[26,27] Under pathological conditions EndMT drives transdifferentiation of normal ECs into mesenchymal cells (eg, fibroblast-like cells, myofibroblasts, or SMCs) with enhanced proliferation, migration, and production of extracellular matrix (ECM). EndMT-derived fibroblast-like cells accumulate prominently in atherosclerotic lesions, contributing to regulation of inflammation, ECM deposition, and plaque instability.[19] Because increased expression of H19[3-5,8,28] and TET1[14] have been detected in diseased/injured blood vessels, a possibility of molecular interplay between H19 and TET1 exists in regulation of EndMT.

Endothelial TGF-β signaling plays a key role in initiation and progression of EndMT, although TGF-β alone is not sufficient to induce EndMT.[18,19,24,25,29] The canonical components of the TGF-β signaling pathway include the TGF-β ligand, TGF-β receptor 2 (TGFBR2), and 1 (TGFBR1), and Smad proteins (Smad2, Smad3, and Smad4). TGF-β is secreted in an inactive form that is activated by a variety of mechanisms including proteolytic cleavage by thrombospondin 1 (TSP1) (reviewed in 30). Active TGF-β binds to TGFBR2, which in turn recruits and activates TGFBR1. Activated TGFBR1 phosphorylates Smad2/Smad3 which then complex with Smad4 and move into the nucleus, where they drive transcription of gene networks promoting epithelial-to-mesenchymal transition (EMT) and EndMT (reviewed in 29,31). The critical role of TSP1 in promoting TGF-β signaling and EndMT is underscored by the notion that TSP1 is present in human atherosclerotic plaques and that its increased expression has been associated with activated or injured endothelium.[32-34] Further, intra-arterial delivery of TSP1 antibodies accelerates re-endothelialization and reduces neointima formation in balloon-injured rat carotid arteries.[35] In addition, *Tsp1*$^{-/-}$ mice show decreased neointima formation following carotid artery ligation.[36] It remains to be tested whether H19/TET1 regulates TGF-β signaling in ECs.

In this report, we identify a novel regulatory pathway encompassing H19 and TET1 that regulates TGF-β signaling in ECs. Using multiple types of primary ECs from both human and mouse, we provide mechanistic evidence that this regulatory pathway promotes EndMT known to play an important role in the pathogenesis and progression of various forms of CVD.

2 | MATERIALS AND METHODS

2.1 | Materials

Antibodies for TET1 (GeneTex, GTX124207; used at a dilution of 1/500 in Western blot and 1:50 in immunofluorescence [IF]), TGFBR2 (Abcam, ab184948; used at a dilution of 1/1000 in WB), TSP1 (Abcam, ab85762; used at a dilution of 1/500 in WB), pSMAD2 (Cell Signaling, 3101; used at a dilution of 1/500 in WB), SLUG (Cell Signaling, C19G7; used at a dilution of 1/500 in WB), SM22α (Novus Biological, NBP1-33003; used at a dilution of 1/50 in WB), Vimentin (Abcam, ab92547; used at a dilution of 1/000 in WB and 1:100 in IF), Fibronectin (Abcam, ab194395; used at a dilution of 1/1000 in WB), CD31 (M0823, Dako; used at dilution of 1:100 in IF), and GAPDH (Abcam, ab128915; used at a dilution of 1/10 000) were purchased. Human H19 expression vector (pH19), H19 siRNA (siH19, 4390771/n272452, Thermo Fisher Scientific), and control siRNA (siCon, 4390843, Thermo Fisher Scientific) were previously described.[37] siTET1 (4390771/n368213, Thermo

Fisher Scientific) and siTET1b (4392420/s199104, Thermo Fisher Scientific) target two different regions of human TET1. pTET1 (FH-TET-pEF)[38] was a gift from Anjana Rao (Addgene plasmid #49792). Recombinant human TNF-α (R&D Systems, 210-TA), IL-1β (R&D Systems, 201-LB), D-glucose (Sigma, G5767), L-glucose (Sigma, G5500), and L-homocysteine (Sigma, 69453) were purchased. TNF-α and IL-1β were reconstituted in 0.1% (w/v) BSA (Sigma, A9647-100G)/phosphate-buffered saline (PBS); glucose and homocysteine (Hcy) were dissolved in water. To made palmitate solution, sodium palmitate (Sigma, P9767) was dissolved in 50% (v/v) ethanol at 37°C, followed by dilution at 37°C in endothelial basal medium EBM-2 (Lonza, CC-3156) supplemented with 1% of BSA to 0.25 mM and 0.5 mM final concentrations, which were within the range of fasting total plasma free fatty acids (0.2-0.8 mM) observed in human nonalcoholic steatohepatitis.[39]

2.2 | Animal work

All animal experiments were performed in accordance with the National Institutes of Health Guidelines on the Use of Laboratory Animals. The Yale University Institutional Animal Care and Use Committee approved the study protocol. The WT and H19 KO mice on a background of C57BL/6J were gifts from Dr Luisa Dandolo (Institut Cochin, Paris, France). All mice used in this study were male. Mice used for the experiments were caged with blinded identity and random orders. Mice were housed at 22-24°C with a 12 hours light/12 hours dark cycle with regular chow (Harlan Teklad no. 2018, 18% calories from fat) and water provided ad libitum. Type 1 diabetes was induced in 13-week old mice by intraperitoneal injection of 50 mg/kg body weight streptozotocin (STZ, Cat. 572 201, EMD Millipore Corporation, USA) daily for 5 days. Blood glucose was monitored weekly. After two consecutive readings of >250 mg/dL (Breeze; Bayer Health Care LLC, Mishawaka, IN), mice were considered diabetic. Pulmonary ECs were collected after 5 weeks of initial STZ injection. Mice were sacrificed using CO2 inhalation.

2.3 | Isolation of pulmonary ECs

Primary mouse pulmonary ECs were isolated with rat anti-mouse CD31 antibody (clone MEC 13.3, Pharmingen, # 553370) conjugated to Dynabeads (catalog number 110.35, Invitrogen) using a protocol similar to that previously described.[40] Briefly, lungs were harvested and minced finely using scissors. Minced tissues were digested with 1 mg/mL of C/D solution (Collagenase/Dispase, #11097113001, Roche) in 15 m of DMEM (one lung per 15 mL) for 45 minutes at 37°C on a rotator. Digestion was stopped by adding 15 mL of IM (Isolation Media, containing 20% FBS and 1× penicillin/streptomycin in DMEM). Digested tissues were triturated 20 times with an 18G cannula attached to a 20 mL of syringe to obtain a single cell suspension which was subsequently passed through a 70 μm cell strainer. Cells were pelleted by centrifugation at 400 *g* for 5 minutes and plated on tissue culture plastic for 1 hours to allow for the adhesion of fibroblasts but not ECs. The unattached cells were then collected and resuspended in 3 mL of 0.1% BSA/PBS, followed by incubation with 22.5 μL of anti-CD31-antibody-coated Dynabeads at room temperature (RT) for 20 minutes on a rotator. After incubation, beads were washed with 1 mL of 0.1% BSA/PBS for 5 times using a magnetic separator. The purified cells were used for RNA and protein analysis.

2.4 | Luciferase assays

psiCHECK2-let-7 4× (Addgene plasmid 20930) was previously described.[41] psiCHECK2-TET1 was created by inserting a 301-bp long fragment (nt 5600-5900, relative to the transcriptional start site of human TET1 [NM_030625.3] that contains three predicted let-7 binding sites) into psiCHECK2-let-7 4x opened with XhoI and NotI (the 4× let-7 binding sites were removed prior to the ligation). Luciferase assays were performed in a 48-well plate scale. Briefly, 20 ng of the indicated luciferase reporter plus 130 ng of empty vector were transfected into human U-2 OS cell line (92022711, Sigma Aldrich) (2×10^5 cell/well), together with negative control miRNA (Con), let-7b, or miR-133 miRNA at a final concentration of 15 or 30 nM. The luciferase reporter plasmid is predicted not to contain miR-133 binding sites. Each concentration was run in triplicate. Luciferase activities were measured 18 hours post-transfection using Promega Dual-Luciferase Reporter Assay System (E1960) according to the manufacturer's protocol. *Renilla* luciferase activity was normalized against Firefly luciferase (FFL) activities and presented as percentage of inhibition.

2.5 | Cell culture, cytokine treatment, and transfection

HUVECs (Lonza, CC-2517) and HAoECs (Lonza, CC-2535) were maintained in a growth medium (GM) composed of EBM-2 supplemented with EGM-2 MV BulletKit (CC-4147, Lonza). Cells were used between passages P2-P5. For cytokine or Hcy treatment, cells were incubated in EBM-2 for 24 hours in the presence of vehicle, TNF-α, TNF-α plus IL-1β, or Hcy at the indicated concentrations. For glucose (D-glucose) or palmitate treatment, cells were first incubated

in EBM-2 for 4 hours, and then, in GM (omitting FBS) for 24 hours in the presence of vehicle, D-glucose, L-glucose (for osmotic control), or palmitate at the indicated concentrations. RNAs were isolated for RT-qPCR analysis.

Cells were transfected in a 24-well plate scale. To prepare siRNA transfection solution for each well, 10 pmol of siCon, siH19, or siTET1 were mixed with 25 μL of OPTI-MEM by gentle pipetting. In parallel, 1 μL of Lipofectamine 3000 was mixed with 25 μL of OPTI-MEM. Following 5 minutes of incubation at RT, the two were mixed by gentle pipetting and incubated for 10 minutes at RT to allow siRNA/lipid complexes to form. At the end of incubation, the 50 μL of transfection solution was used to resuspend cell pellet (3×10^4 cells/well). After incubation at RT for 10 minutes, GM was added at a ratio of 1:9 (1 volume of transfection solution/9 volumes of GM) and the cell suspension was transferred to a culture plate. For TNF-α treatment combined with H19 knockdown, cells were transfected with siCon or siH19 for 24 hours, followed by addition of TNF-α at a final concentration of 10 ng/mL for an additional 24 hours before RNA extraction. For iLet 7 rescue experiments, 10 pmol of siCon + iCon, iCon + siH19, or siH19 + iLet7 were used for each well of 3×10^4 cells. Forty-eight hours after the transfection, RNA and protein were extracted for analysis.

To prepare DNA/lipid complexes for pH19/pTET1 overexpression or pTET1 overexpression rescue experiments, empty vector (0.5 μg), pH19 (0.5 μg), or pTET1 (0.75 μg) were mixed with 1 μl of P3000 in 25 μL of OPTI-MEM by gentle pipetting. In parallel, 0.75 μL of Lipofectamine 3000 was mixed with 25 μl of OPTI-MEM. The contents in the two tubes were mixed by gentle pipetting and incubated at RT for 5 minutes. The resulting DNA/lipid complexes (50 μL) were added to one well of cells (8×10^4), which had been seeded in a 24-well plate in GM the night before. Following incubation at RT for 10 minutes, 300 μL of OPTI-MEM was added and cells were incubated in a tissue culture incubator for 4-6 hours. Subsequently, 500 μL of GM was added and cells were incubated in a tissue culture incubator overnight. The next day, the medium was replaced with fresh GM. For pTET1 overexpression rescue experiments, the indicated pTET1/lipid complexes and siH19/lipid complexes were prepared separately, and then, pooled to one well of 8×10^4 cells seeded the night before in a 24-well plate. Forty-eight hours after the transfection, RNA and protein were extracted for analysis.

2.6 | Chromatin immunoprecipitation-quantitative PCR (ChIP-qPCR)

Experiments were performed in a 10-cm dish scale using the Pierce Agarose ChIP Kit (Thermo Scientific, 26156) according to the manufacturer's instructions with minor modifications. Briefly, agarose beads were used to pre-binding overnight with antibodies against TET1 (Millipore Sigma, ABE1034), H3K4me3 (Cell signaling, C42D8), and H3K27me3 (Cell signaling, C36B11). IgG was included as a negative control. Cells were cross-linked with 1% of formaldehyde at RT for 10 minutes, and the reaction was stopped by 1× glycine. ChIPs were carried out overnight at 4°C. Primers (Table S1) for the promoter regions of TGFBR2 and TSP1 were used to amplify input and ChIP-purified DNA. The relative enrichments of the indicated DNA regions were calculated using the Percent Input Method according to the manufacturer's instructions and were normalized to % input.

2.7 | Quantitative methylation-specific PCR

Genomic DNA was extracted from HUVECs in one well of 24-well plates using Quick-gDNA MicroPrep (Zymo Research Corporation, Irvine, CA; D3021) according to the manufacturer's instructions. For bisulfite treatment, 200 ng of DNA was used for each column using EZ DNA Methylation-Gold Kit (Zymo, D5006). About 100 μL of elution buffer was used to elute DNA from each column. Real-time quantitative PCR was performed in a 15 μL reaction containing 5 μL of the eluted DNA using iQSYBRGreen (Bio-Rad, Hercules, CA; 1708880) in a Bio-Rad iCycler. Two sets of PCR primers were designed: one for unmethylated and one for methylated DNA sequences (Table S1). The PCR primers for methylated DNA were used at a final concentration of 0.6 μM in each PCR reaction. PCR was performed by initial denaturation at 95°C for 5 minutes, followed by 40 cycles of 30 seconds at 95°C, 30 seconds at 60°C, and 30 seconds at 72°C. Specificity was verified by melting curve analysis and agarose gel electrophoresis. The threshold cycle (Ct) values of each sample were used in the post-PCR data analysis. The ratio of methylated versus unmethylated DNA sequences are presented.

2.8 | Serum TNF-α analysis

Blood samples were collected by retro-orbital sinus puncture after 2 weeks of initial STZ injection via the medial cants of the eye using clean 100 μL of VWR Disposable Micropipets (Cat. 53432-921, VWR). After incubation on ice for 30 minutes, serum was obtained through centrifugation of the blood for 20 minutes at 3000 *g* at 4°C and stored at –80°C until use. Serum TNF-α measurements were performed using Luminex assays according to the manufacturers' protocols. Briefly, wells of a 96-well filter plate were loaded with either 50 μL of standard solution or 50 μL of serum and incubated with

a mouse 23plex ProBead mix from BioRad (#m60009rdpd Bio-Rad Laboratories) at ±800 rpm for 30 minutes in the dark RT. Wells were then vacuum-washed three times with 100 μL of wash buffer. Samples were then incubated with 25 μL of biotinylated detection antibody at ±800 rpm for 30 minutes at RT in the dark. After three washes, 50 μL of streptavidin-phycoerythrin was added to each well and incubated for 10 minutes at ±800 rpm at RT in the dark. After a final wash, the beads were resuspended in 125 μL of sheath buffer for measurement using the LUMINEX 200 (LUMINEX, Austin, TX, USA).

2.9 | IF and RNA in situ hybridization

These experiments were performed on specimens derived from the same patient cohort.[18] The procedures related to human subjects were approved by the Institutional Review Boards of Yale University and by the New England Organ Bank. Human coronary arteries were obtained from the explanted hearts of transplant recipients or cadaver organ donors. Detailed specimen acquisition and information on the specimens were described previously.[18] All experiments were performed on frozen specimens in Optimal Cutting Temperature Medium (Sakura Finetek USA Inc). IF experiments were performed using our previously described protocols.[18] Briefly, frozen tissue sections cut at 5-μm were washed 5 minutes × 3 and incubated with primary antibodies diluted in blocking solution (10% BSA and 5% horse serum in 1xPBS) overnight at 4°C in a humidified chamber. Sections were washed for 10 minutes × 3 with 1xPBS, followed by incubation with second antibodies conjugated with Alexa Fluor 488 or Alexa Fluor 647 (diluted at 1:500 in blocking solution) for 1 hour at RT. Sections were washed again for 10 minutes × 3 with 1 × PBS, stained with DAPI (Vector Lab, Burlingame, CA, diluted at 1:1000) for 5 minutes, and mounted with VECTASHIELD Mounting medium (H-1000). Images were obtained using the fluorescence microscopy system (KEYENCE BZ-X710) at a magnification of 40×. Image J was used for quantification. Measurements were made of the intima (I) and media (M) thickness. The I/M ratio was used to grade the atherosclerosis severity. Coronary arteries with an I/M ratio of less than 0.2 were considered as no disease or mild disease; those with an I/M ratio of 0.2 to 1 were considered as moderate disease; those with an I/M ratio of greater than 1 or with calcification were considered as having severe disease. Parameters in IF were assessed and averaged to obtain mean values from four different areas for each specimen. NIH ImageJ was used to measure neointima thickness and cells. Neointima or intima and media thickness were measured and averaged in four different areas for each section along a cross and from five serial cross-sections 150 μm apart per specimen. FN1+/CD31+ or VIM+/CD31+ or TET1+/CD31+ cells were analyzed for colocation of endothelial markers and End-MT markers in at least 10 sections 150 μm apart per specimen imaged under 40× magnification.

For H19 and CD31 RNA colocolization, in situ hybridization (ISH) experiments were performed on 5-μm frozen sections using the RNAscope 2.5 HD Duplex Reagent Kit (Advanced Cell Diagnostic Inc, 322500) according to the manufacturer's instructions. The system included the following components: Hs-H19 probe (P/N: 400771), Hs-PECAM-1 probe (P/N: 487381), Hs-Positive Control probe (P/N: 321641), 2-Plex Negative Control probe (P/N: 320751), Pretreatment Kit with protease IV (P/N: 322336), and Detection Kit (P/N: 322500). Briefly, samples were fixed with 4% of formaldehyde for 2 hours at RT, followed by protease IV digestion for 30 minutes to remove proteins including nucleases. The previously characterized H19 probe[42,43] and CD31 probe were mixed and added to the slides to hybridize for 2 hours at 40°C in a HybEz oven (Advanced Cell Diagnostic Inc), followed by signal amplification and washing steps, and mounted with VECTASHIELD Mounting medium (H-5000). Hybridization signals were detected by red and green chromogens for CD31 and H19, respectively. Images were acquired using the microscopy system (KEYENCE BZ-X710) in bright field mode.

2.10 | RNA extraction and RT-qPCR

Total RNAs were extracted using PureLink RNA Mini Kit (Ambion, catalog number 12183018A). cDNA was synthesized using PrimeScript RT Reagent Kit (TAKARA, RR037A) in a 20 μL reaction containing 0.5-1 μg of total RNA. Real-time quantitative PCR was performed in a 15 μL reaction containing 0.5-1 μL of cDNA using iQSYBRGreen (Bio-Rad) in a Bio-Rad iCycler. PCR was performed by initial denaturation at 95°C for 5 minutes, followed by 40 cycles of 30 seconds at 95°C, 30 seconds at 60°C, and 30 sec at 72°C. Specificity was verified by melting curve analysis and agarose gel electrophoresis. The Ct values of each sample were used in the post-PCR data analysis. Gene expression levels were normalized against GAPDH. Real-time PCR primers are listed in Table S1.

2.11 | Western blot analysis

HUVECs in 24-well plates were dissociated with 0.25% of trypsin. Cell pellets were collected by centrifugation at 1000 rpm for 5 minutes. Cell pellets were homogenized in 2× sodium dodecyl sulfate (SDS)-sample buffer (100 μL/well), followed by heating at 100°C for 5 minutes, with occasional vortexing. Homogenized samples were loaded onto 12% of SDS gel (5 μL/well), followed by Western blot analysis.

Bands on Western blot gels were quantified using ImageJ. GAPDH was used as a loading control. For pulmonary ECs, 2x SDS-sample buffer was used to homogenize the cells (50 μL/mouse). For detection of multiple proteins using a single GAPDH control, blots were cut in pieces according to protein size and probed with respective antibodies separately.

2.12 | Let-7 binding sites prediction

The RNAhybrid program[44] (https://bibiserv2.cebitec.uni-bielefeld.de/rnahybrid?id=rnahybrid_view_submission) was used to predict let-7 binding sites in TET1 mRNA.

2.13 | Statistical analysis

Statistical analyses and figure construction were performed using GraphPad Prism version 7.01 for Windows (GraphPad Software, La Jolla California USA, www.graphpad.com). Data are presented as mean ± standard error of the mean (SEM). All data except indicated otherwise in the figure legends were analyzed using two-tailed Student *t* test. Kolmogorov-Smirnov test indicated a normal data distribution, a prerequisition for Student *t* test (data not shown). *P* values at .05 or smaller (two-sided) were considered statistically significant.

2.14 | Data and resource availability

The data sets generated during and/or analyzed during the current study are available from the corresponding author upon reasonable request.

3 | RESULTS

3.1 | Endothelial expression of H19 and TET1 associates with human atherosclerosis

We have previously documented that the extent of coronary artery disease (CAD) in patients strongly correlated with endothelial activation of TGF-β signaling and the extent of EndMT.[18] In this previous report, IF studies on human left main coronary arteries with normal coronaries (no neointima), mild CAD (intima-to-media [I/M] ratio < 0.2, grade I plaque), moderate CAD (I/M ratio 0.2-1.0, grade II plaque), or severe CAD (I/M ratio > 1.0, grade III and IV plaque) were conducted. Significantly increased expressions of p-SMAD2 (a marker of activated TGF-β signaling) and NOTCH3, SM22-α, collagen 1, and fibronectin 1 (markers of EMT and EndMT) in luminal coronary ECs were detected in CAD, with a strong positive linear relationship between the I/M ratio and number of ECs expressing the markers.[18]

To explore the potential clinical significance of H19 and TET1 expression in CAD, we performed RNA ISH and IF studies on left main coronary arteries derived from the same patient cohort.[18] While essentially no luminal coronary ECs in patients with no/mild CAD expressed H19, this was increased to 12% of the luminal endothelium in patients with moderate CAD and 26% in patients with severe CAD (Figure 1A,B, and Figure S1). There was a strong positive correlation between the I/M ratio and number of ECs expressing H19 ($r = .75$, $P = .001$, Figure 1B). In the same samples, no TET1 expression was detected in patients with no/mild CAD, but TET1 express increased to 25% and 46% of the luminal endothelium in patients with moderate and severe CAD, respectively (Figure 1, C and D). Further, there was a strong linear relationship between the I/M ratio and number of ECs expressing TET1 ($r = .78$, $P = .0005$, Figure 1D) as well as expression between H19 and TET1 ($r = .86$, $P < .0001$, Figure 1E). Next, we examined the EndMT markers VIM and FN1 in this patient population. Consistent with our previous findings,[18] their expression by the luminal ECs strongly correlated with increasing I/M ratio and disease severity (Figure S2). Moreover, there was a strong positive linear correlation between luminal EC expression of H19 and FN1, H19 and VIM, TET1 and FN1, and TET1 and VIM (Figure 1F). Taken together with previous findings from the same patient cohort demonstrating a strong association between the extend of coronary atherosclerosis and activation of TGF-β signaling and EndMT,[18] these results suggest a possible regulatory pathway involving H19 and TET1 in promoting TGF-β signaling and EndMT.

3.2 | H19 expression is induced by multiple factors associated with endothelial dysfunction and CVD

Inflammation, hyperglycemia, hyperlipidemia, and hyperhomocysteinemia promote endothelial dysfunction and are well-established risk factors for CVD.[45-47] Treatment of human umbilical vein ECs (HUVECs) with inflammatory cytokines TNF-α and IL-1β-induced endothelial inflammation and EndMT ([18,24]). To begin to explore the possible mechanism by which H19 and TET1 regulate ECs, we treated HUVECs with TNF-α. As seen in Figure 2A (and Figure S3A, biological replicates), TNF-α stimulated H19 expression in a dose-dependent manner. Similar results were obtained in primary human aortic endothelial cells (HAoECs) (Figure 2B). We tested additional factors in HUVECs and found that all of them (IL-1β, Hcy, glucose, and palmitate) increased H19 expression (Figure S3B-E).

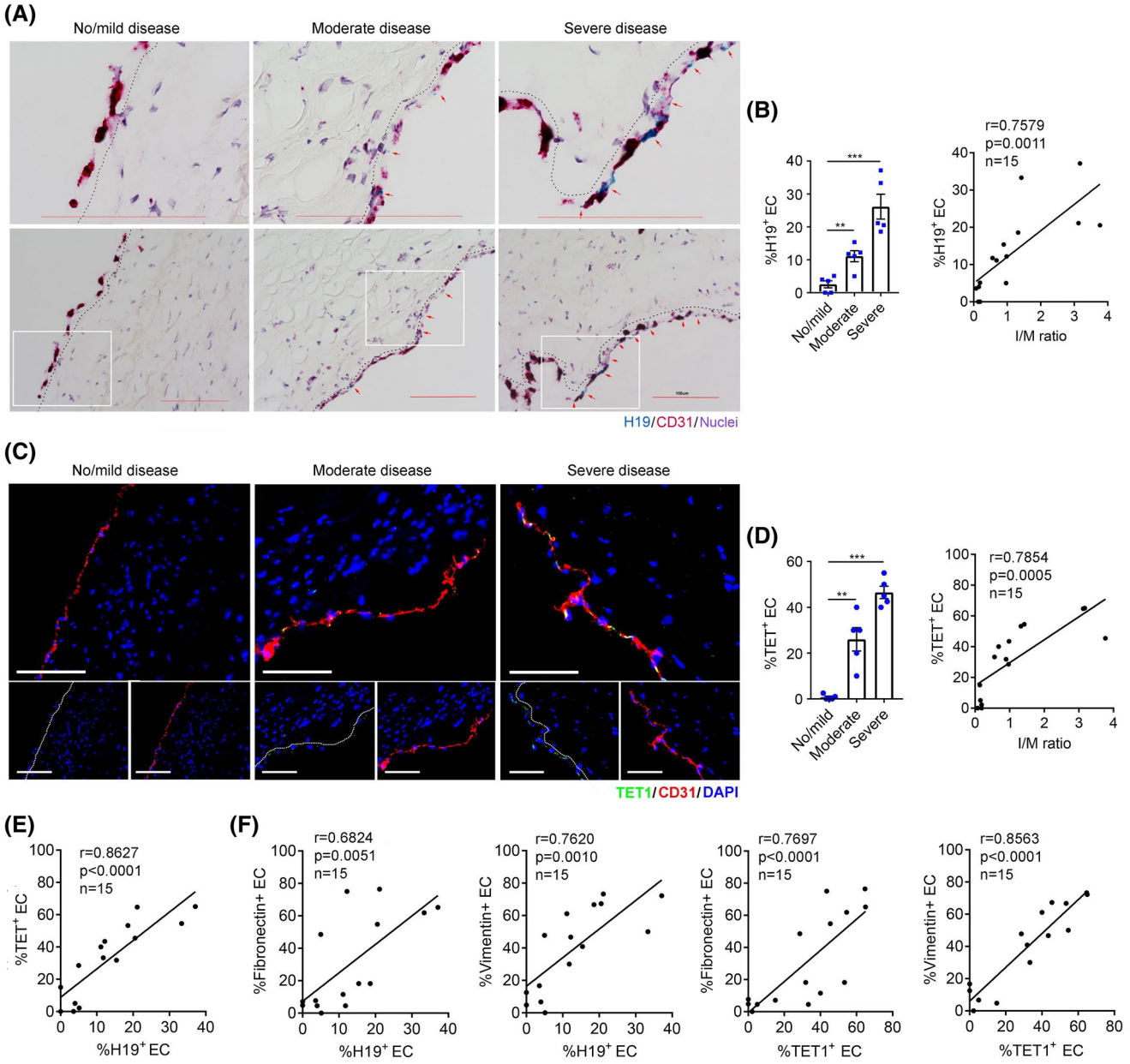

FIGURE 1 H19 and TET1 expression in ECs in human coronary arteries. Left main coronary arteries from patients with no/mild, moderate, and severe CAD were assessed. n = 5 in each group. A, Representative images of RNA ISH staining of left main coronary arteries from patients for H19 (blue) and CD31 (red), with nuclei stained in purple. Note, a fraction of CD31 mRNA is also present in the nucleus which overlaps with the purple nuclear counterstaining. Scale bar: 100 μm. C, Representative images of immunofluorescence staining for TET1 (green) and CD31 (red), with nuclei stained with DAPI in blue. Scale bar: 100 μm. B and D, Left panels: percentage of $H19^+$ ECs or $TET1^+$ ECs in the lumen. $^{**}P < .01$; $^{***}P < .001$ compared with no/mild disease; one-way ANOVA with Newman-Keuls post hoc test for multiple comparison correction. Right panels: scatter plots of $H19^+$ ECs or $TET1^+$ ECs and the I/M ratio. The corresponding Spearman's correlation coefficient (r) between $H19^+$ ECs or $TET1^+$ ECs and the I/M ratio and the *P* value are shown. E, Scatter plot of $H19^+$ ECs and $TET1^+$ ECs. The corresponding Spearman's correlation coefficient (*r*) between $H19^+$ ECs and $TET1^+$ ECs and the *P* value are shown. F, Scatter plots of $H19^+$ ECs and $FN1^+$ ECs; $H19^+$ ECs and VIM^+ ECs; $TET1^+$ ECs and $FN1^+$ ECs; and $TET1^+$ ECs and VIM^+ ECs

3.3 | H19 regulates expression of TET1 and key TGF-β pathway genes

In light of our observation that TET1, TGFBR2, and TSP1 were among the most significantly downregulated genes following H19 knockdown in primary human uterine SMCs (GEO accession number GSE110557), we tested whether H19 regulates these genes in HUVECs. Thus, H19 was downregulated using a previously validated siRNA specific for H19 (siH19,[37]). H19 knockdown reduced expression of TET1, TGFBR2, and TSP1 (Figure 2C). In contrast, H19 overexpression by transfection of a human H19-expression vector pH19 ([37,48]) increased

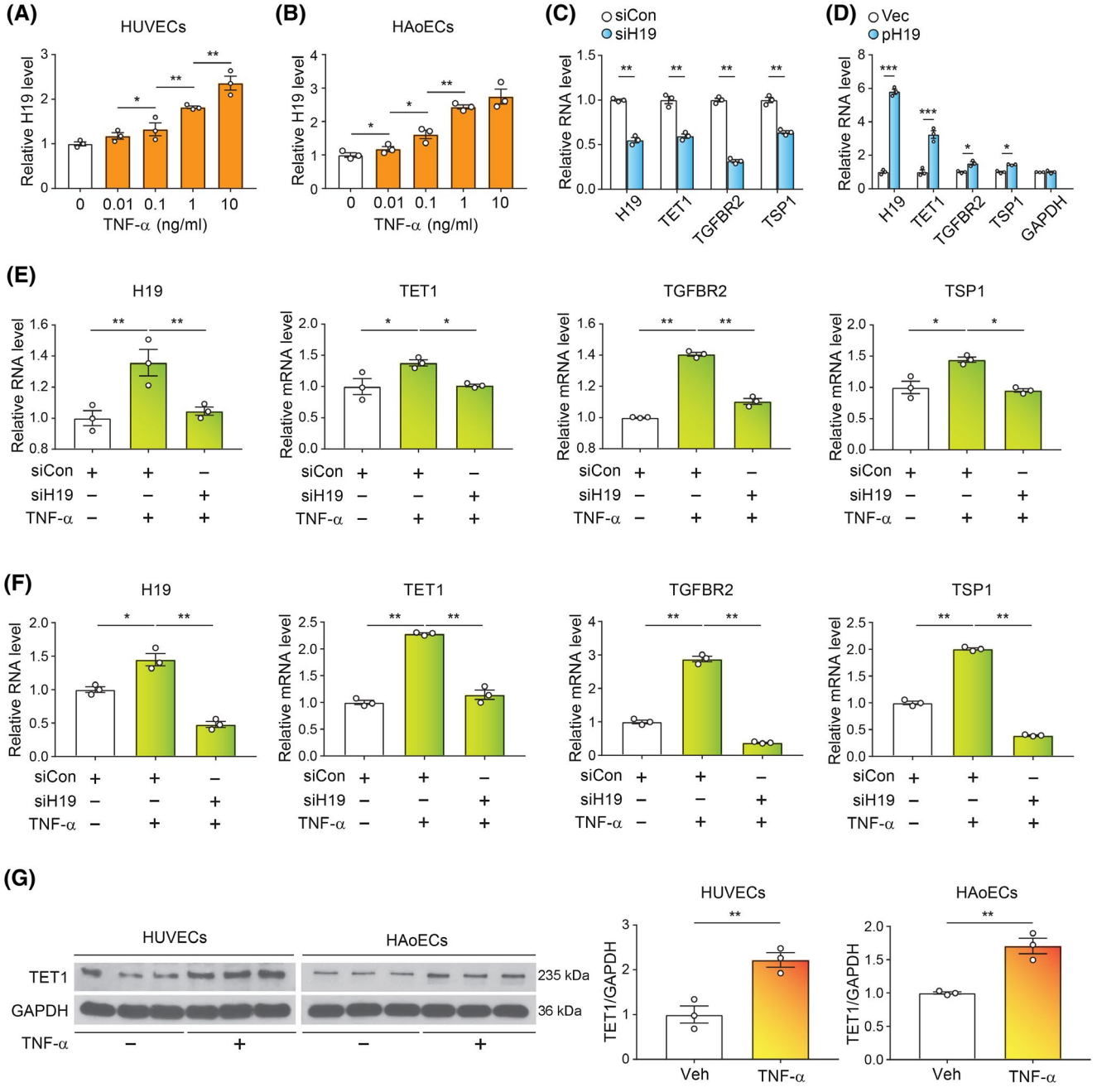

FIGURE 2 TNF-α upregulates endothelial expression of H19 and TGF-β signaling genes in a H19-dependent manner. RT-qPCR analysis of H19 in TNF-α-treated (overnight) HUVECs (A) or HAoECs (B). One-way ANOVA with Newman-Keuls post hoc test. C, RT-qPCR analysis of H19, TET1, TGFBR2, and TSP1 48 hours after transfection of HUVECs with control siRNA (siCon) or H19-specific siRNA (siH19). D, RT-qPCR analysis of the indicated genes 48 hours after transfection of HUVECs with empty vector (Vec) or human H19-expressing plasmid (pH19). E and F, RT-qPCR of H19, TET1, TGFBR2, and TSP1 following transfection of siCon (-) or siH19 (+) for 24 hours and treatment with TNF-α (10 ng/mL) (+) or vehicle (-) for an additional 24 hours in HUVECs (E) or HAoECs (F). Two-way ANOVA with Newman-Keuls post hoc test. G, Western blots of TET1 following TNF-α treatment of HUVECs or HAoECs. $*P < .05$; $**P < .01$; ns, not statistically significant compared to control. All experiments were performed three times with one set of representative results shown. Error bars were calculated in technical replicate, n = 3

their expression (Figure 2D). Further, TNF-α upregulated expression of TET1, TGFBR2, and TSP1, which was abrogated when H19 was downregulated (Figure 2E). Similar results were obtained with HAoECs (Figure 2F). Importantly, TNF-α-induced upregulation of TET1 was further confirmed at the protein level (Figure 2G). These results suggest that H19 positively regulates expression of TET1, TGFBR2, and TSP1 in ECs and that TNF-α upregulates these genes in a H19-dependent manner. We decided to focus on H19-mediated regulation of TET1, TGFBR2, and TSP1 in ECs in the present study although it is highly likely that H19 affects other gene expression as well, which warrant future investigation.

3.4 | H19 regulates TET1 expression via the H19/let-7 axis

We have previously documented that H19 acts as a molecular sponge for microRNA let-7.[37] Both human and mouse H19 contains multiple binding sites for let-7; binding of H19 to let-7 sequesters let-7 and prevents it from inhibiting target gene expression (hence, H19 functions to reduce the bioavailability of let-7).[7,37,48-50] Binding of let-7 to complementary sequences in target mRNAs results in translational repression and/or mRNA degradation.[51] Thus, it is the relative expression levels of H19 and let-7 (rather than their absolute expression levels) that determine the outcome of let-7 target gene expression. First, we sought to determine how H19 regulates TET1. We performed bioinformatics analysis and predicted multiple let-7-binding sites in both human and mouse TET1 mRNAs, with the binding sites concentrated in the open reading frame (Figure 3A). This suggested that H19 may promote TET1 expression by sequestering let-7. To test this possibility, we used a previously reported methodology to perform H19 knockdown experiments in combination with a let-7-specific inhibitor (iLet7) or anti-miR control (iCon as negative control)[7,48-50,52] in HUVECs cells. iLet7 are chemically modified, single-stranded nucleic acids that specifically bind to let-7 and block its activity. The effect of H19 knockdown (ie, downregulation of TET1) was expected to be abrogated in the presence of iLet7, which acts to neutralize let-7 released from H19 sequestration.[7,48-50,52] Indeed, H19 knockdown resulted in decreased TET1 expression at both the mRNA (Figure 3B) and protein (Figure 3C) levels and the expression was restored to control levels in the presence of iLet7.

To confirm the functionality of three predicted let-7 binding sites in human TET1, positions 5604, 5613, and 5922 (Figure 3A), experiments using let-7 biosensors were conducted. psiCHECK2-let-7 4×[41] harbors four copies of let-7 binding sites in the 3′-UTR of a Renilla luciferase (Rluc) gene (Figure 3D). This construct also contains a constitutively expressed FFL gene as an internal control for normalization. In psiCHECK2-TET1, the four copies of let-7 binding sites were replaced with a 301-bp fragment containing three predicted let-7 binding sites from human TET1 (Figure 3D). Co-transfection of let-7b inhibited Rluc activity in a dose-dependent manner for both psiCHECK2-TET1 and psiCHECK2-let-7 4×, while co-transfection of miR-133 did not affect Rluc activity of psiCHECK2-let-7 4× which was predicted not to contain miR-133 binding sites (Figure 3D), suggesting that positions 5604, 5613, and 5922 contain functional let-7 binding sites. Altogether, these results demonstrate that TET1 is a novel target of let-7 and that H19 regulates TET1 expression posttranscriptionally via decreasing the bioavailability of let-7.

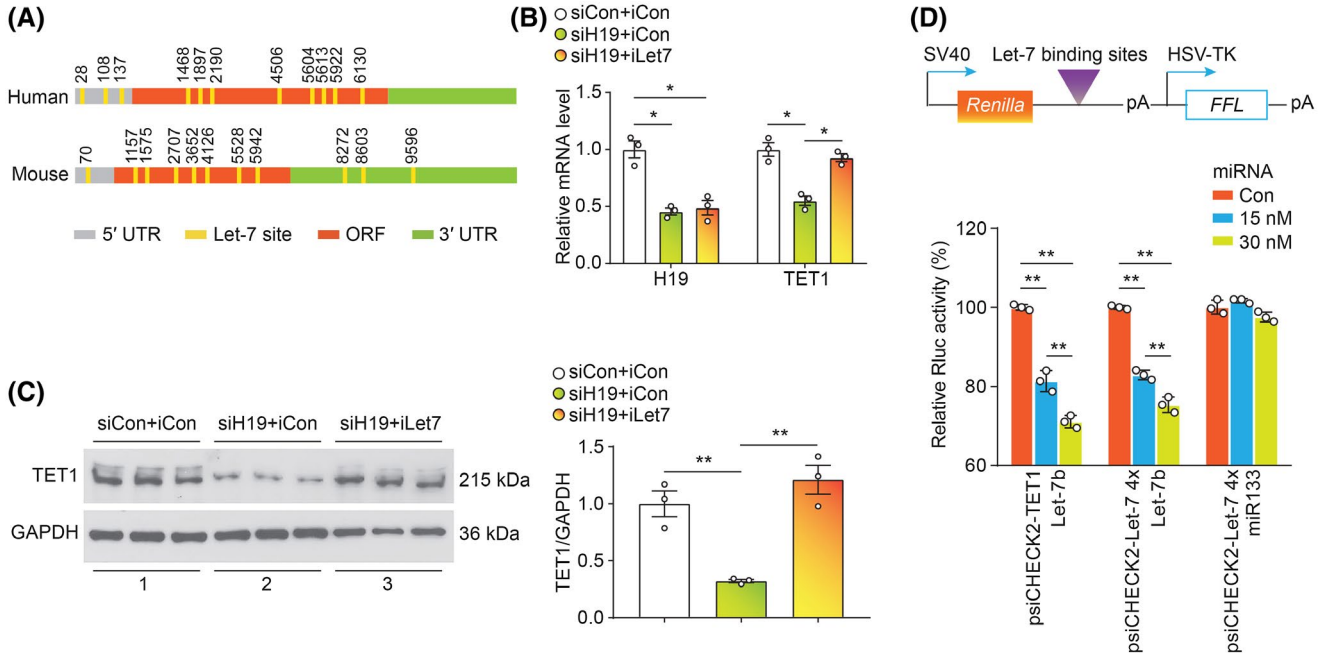

FIGURE 3 H19 regulates TET1 expression posttranscriptionally via reducing the bioavailability of let-7. A, Schematics of human and mouse TET1 mRNAs, with numbers on top depicting positions of let-7-binding sites relative to the transcriptional start sites. Figures are not drawn to scale. B and C, HUVECs were transfected with a mixture of siCon and iCon, siH19 and iCon, or siH19 and iLet7. RNA and protein were isolated 48 hours later and analyzed by RT-qPCR (B) and Western blot (C). In C, protein samples were loaded in triplicate, with quantification of TET1 protein shown on the right. GAPDH was used as a loading control. D, Top, reporter constructs; bottom, the indicated constructs were each transfected into U-2 OS cells, together with control miRNA (Con), let-7b, or miR-133 at a final concentration of 15 or 30 nM. $*P < .05$; $**P < .01$. One-way ANOVA with Newman-Keuls post hoc test. All transfection experiments were carried out three times with one set of representative results shown. Error bars were calculated in technical replicate, n = 3

3.5 | TET1 regulates expression of TGFBR2 and TSP1 at the epigenetic level

TET2, which normally expresses in mature SMCs, acts to promote key pro-contractile gene expression at the epigenetic level. Mechanistically, TET2 binds to target gene promoters and modifies histones at these promoters, leading to transcription activation.[11] In light of these previous findings, we asked whether TET1 regulates gene expression in a similar manner. Thus, we knocked down TET1 in HUVECs using a TET1-specific siRNA (siTET1) and observed decreased expression of TGFBR2 and TSP1 both at the mRNA (Figure 4A) and protein (Figure 4B) levels without affecting H19 expression, suggesting that TET1 positively regulates expression of TGFBR2 and TSP1. TET1 knockdown did not affect TET2 and TET3 expression (Figure S4A). The specificity of the siTET1 was further confirmed by using a different TET1 siRNA

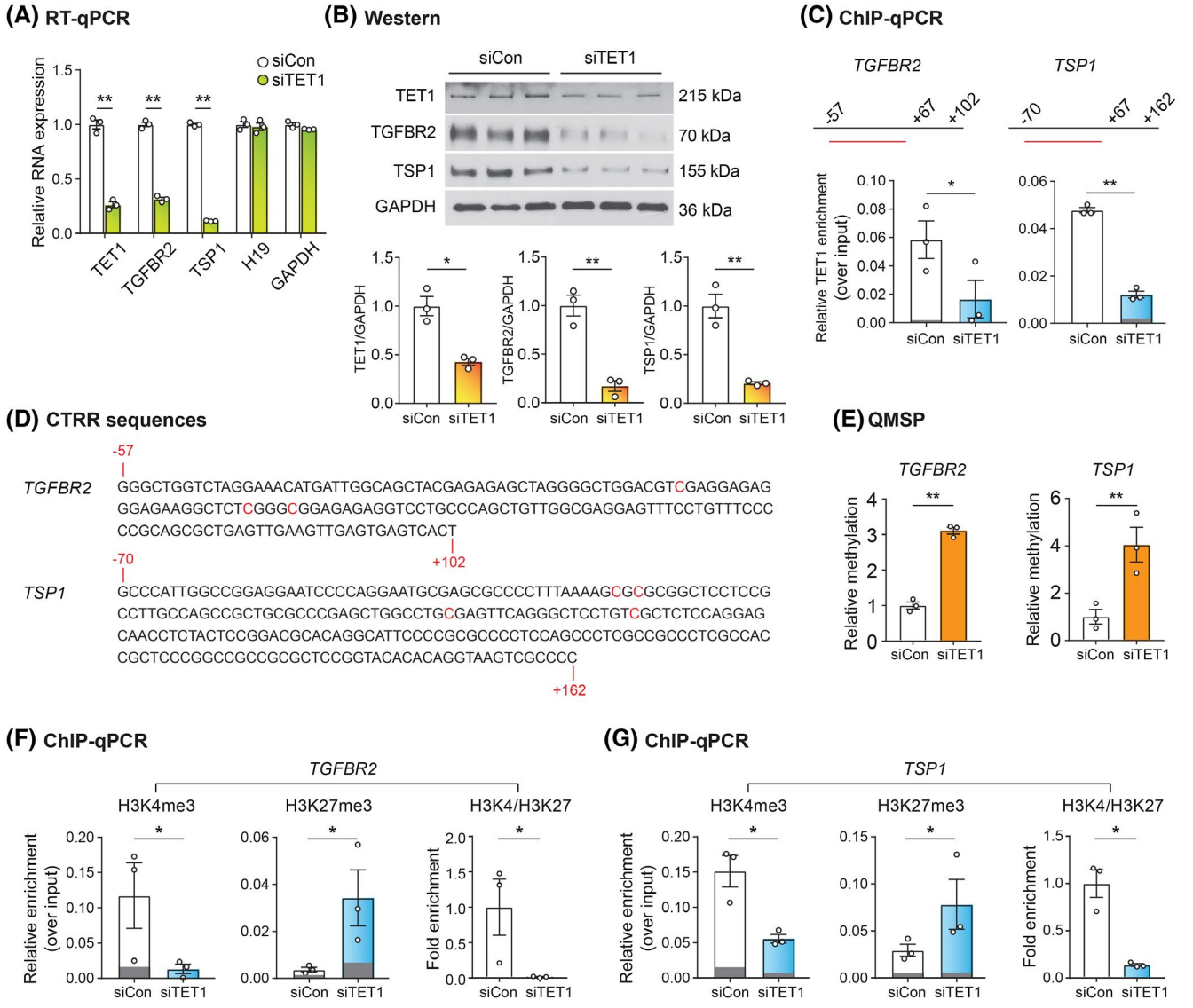

FIGURE 4 TET1 affects promoter methylation and histone modifications of TGFBR2 and TSP1. A and B, HUVECs were transfected with siCon or siTET1. RNA and protein were isolated 48 hours later and analyzed by RT-qPCR (A) and Western blot (B). In B, protein samples were loaded in triplicate, with quantification of TGFBR2 and TSP1 proteins shown on the bottom. C, HUVECs were transfected with siCon or siTET1, followed by ChIP-qPCR analysis. Data are presented as mean relative TET1 enrichment over input, with gray bars representing background IgG signal. Numbers indicate nucleotide positions relative to the transcriptional start sites, with PCR products depicted as red bars underneath. D, Sequences of critical transcription regulatory regions (CTRR) of TGFBR2 and TSP1. The differentially methylated cytosine residues are marked in red. The red numbers mark the positions of the indicated nucleotides relative to the transcriptional start sites. E, HUVECs were transfected with siCon or siTET1 for 48 hours, followed by QMSP analysis. F and G, HUVECs were transfected with siCon or siTET1 for 48 hours, followed by ChIP-qPCR analysis. *$P < .05$; **$P < .01$; ns, not statistically significant compared to control. All transfection experiments were performed three times with one set of representative results shown. Error bars were calculated in technical replicate, n = 3

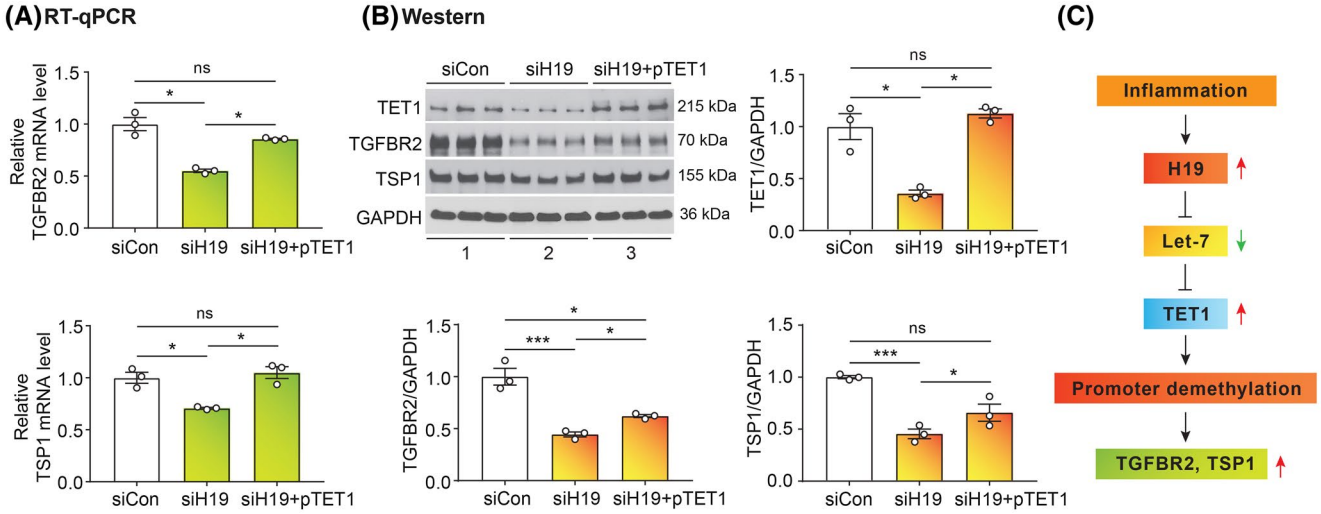

FIGURE 5 H19 regulates TGFBR2 and TSP1 expression in a TET1-dependent manner. A, HUVECs were transfected with siCon, siH19, or siH19 plus pTET1 (human TET1-expressing plasmid). RNA and protein were extracted 48 and 72 hours later, respectively, and analyzed by RT-qPCR (A) and Western blot (B). $*P < .05$; $**P < .01$; $***P < .0001$; ns, not statistically significant compared to control. One-way ANOVA with Newman-Keuls post hoc test. All transfection experiments were carried out three times with one set of representative results shown. Error bars were calculated in technical replicate, n = 3. C, A proposed regulatory pathway

(siTET1b) targeted to a different region of human TET1 (Figure S4B).

TET1 most likely also targets other genes; we decided to focus on TGFBR2 and TSP1 in the present study as they are among the most critical upstream genes of TGF-β signaling. Thus, we tested the possibility of a direct interaction between TET1 and the two genes. We performed chromatin immunoprecipitation coupled with qPCR (ChIP-qPCR) experiments using a TET1-specific antibody to immunoprecipitate protein-DNA complexes from HUVECs transfected with siCon or siTET1 and qPCR amplified the critical transcriptional regulatory regions (CTRRs) of the TGFBR2[53] and TSP1[54] promoters. In TET1 knockdown cells, binding of TET1 to the respective promoters was significantly reduced as compared to control cells, consistent with physical interactions of TET1 with the promoters (Figure 4C).

It is well established that TET proteins promote DNA demethylation leading to alteration of chromatin states. First, we tested whether TET1 knockdown alters promoter methylation of TGFBR2 and TSP1. Our genome-wide single-nucleotide resolution DNA methylation studies from human uterine cells following TET3 knockdown showed increased methylation in the CTRRs of the TGFBR2 and TSP1 promoters[55] (Figure 4D). We hypothesized that TET1 knockdown in HUVECs may induce similar methylation changes in the CTRRs of TGFBR2 and TSP1. Thus, quantitative methylation-specific PCR (QMSP) was performed on DNA isolated from HUVECs using our previously described methods.[56,57] The QMSP primers were designed based on the differentially methylated cytosine residues within the CTRRs (Figure 4D, red highlighted cytosines). As seen in Figure 4E, HUVECs treated with siTET1 had an increase in methylation in the CTRRs compared with cells treated with siCon. These results suggest that binding of TET1 to TGFBR2 and TSP1 induces promoter demethylation in HUVECs.

Next, we tested whether TET1 knockdown affects chromatin states of target genes. HUVECs were transfected with siCon or siTET1, followed by ChIP-qPCR, immunoprecipitating with antibodies specific for the H3K4me3 (active) or H3K27me3 (inactive) marks and amplifying the CTRRs of TGFBR2 and TSP1. ChIP analysis showed that TET1 knockdown significantly decreased H3K4me3 (Figure 4F,G, left panels) and increased H3K27me3 (middle panels) association with both gene promoters, such that the ratios of H3K4me3/H3K27 me3 decreased significantly (right panels). These results suggest that TET1 knockdown likely promotes a heterochromatin conformation, diminishing chromatin accessibility at the TGFBR2 and TSP1 promoter regions.

3.6 | The H19/TET1 axis regulates expression of TGFBR2 and TSP1

To test whether H19 regulates TGFBR2 and TSP1 via TET1, HUVECs were transfected with siCon, siH19, or siH19 together with a human TET1 expression vector pTET1.[38] RNA and proteins were analyzed at 48 and 72 hours post-transfection, respectively. H19 knockdown expectedly led to decreased mRNA levels of both TGFBR2 and TSP1 (Figure 5A, compare middle bars to left bars). However, when H19 was knocked down together with TET1 overexpression, the

mRNA levels of TGFBR2 and TSP1 were no longer decreased (Figure 5A, compare right bars to left bars). The ability of TET1 to rescue the effect of H19 knockdown on TGFBR2 and TSP1 expression was further confirmed at the protein level (Figure 5B). The partial rescue of TGFBR2 by TET1 at the protein level (Figure 5B) suggested additional translational/posttranslational regulatory mechanisms which warrant future investigation. Based on our studies in ECs shown above, we propose a pathway illustrated in Figure 5C.

3.7 | H19 and TET1 upregulate TGF-β signaling and EndMT in human ECs in vitro

As H19 positively regulates expression of key TGF-β signaling genes TGFBR2 and TSP1 via TET1, we sought to address whether overexpression of H19 or TET1 increases TGF-β signaling and EndMT marker expression. Thus, HUVECs were transfected with pH19 or pTET1, followed by pathway gene expression analysis. When H19 or TET1 was overexpressed, the expression of TET1, TGFBR2, and TSP1 was expectedly increased (Figure 6A, top three blots; Figure 6B, top three panels on the left; and Figure S5A). There was also an increase in phosphorylation of TGF-β signaling intermediary SMAD2 (p-SMAD2) as well as upregulation of EndMT markers SLUG, smooth muscle 22 alpha (SM22-α), vimentin (VIM), and fibronectin 1 (FN1) (Figure 6A,B, and Figure S5A). Similar results were obtained in HAoECs (Figure 6C,D). Importantly, overexpression of H19 or TET1 also led to decreased expression of vascular endothelial marker VE-cadherin/CD144 (Figure 6C,D, and Figure S5B), which

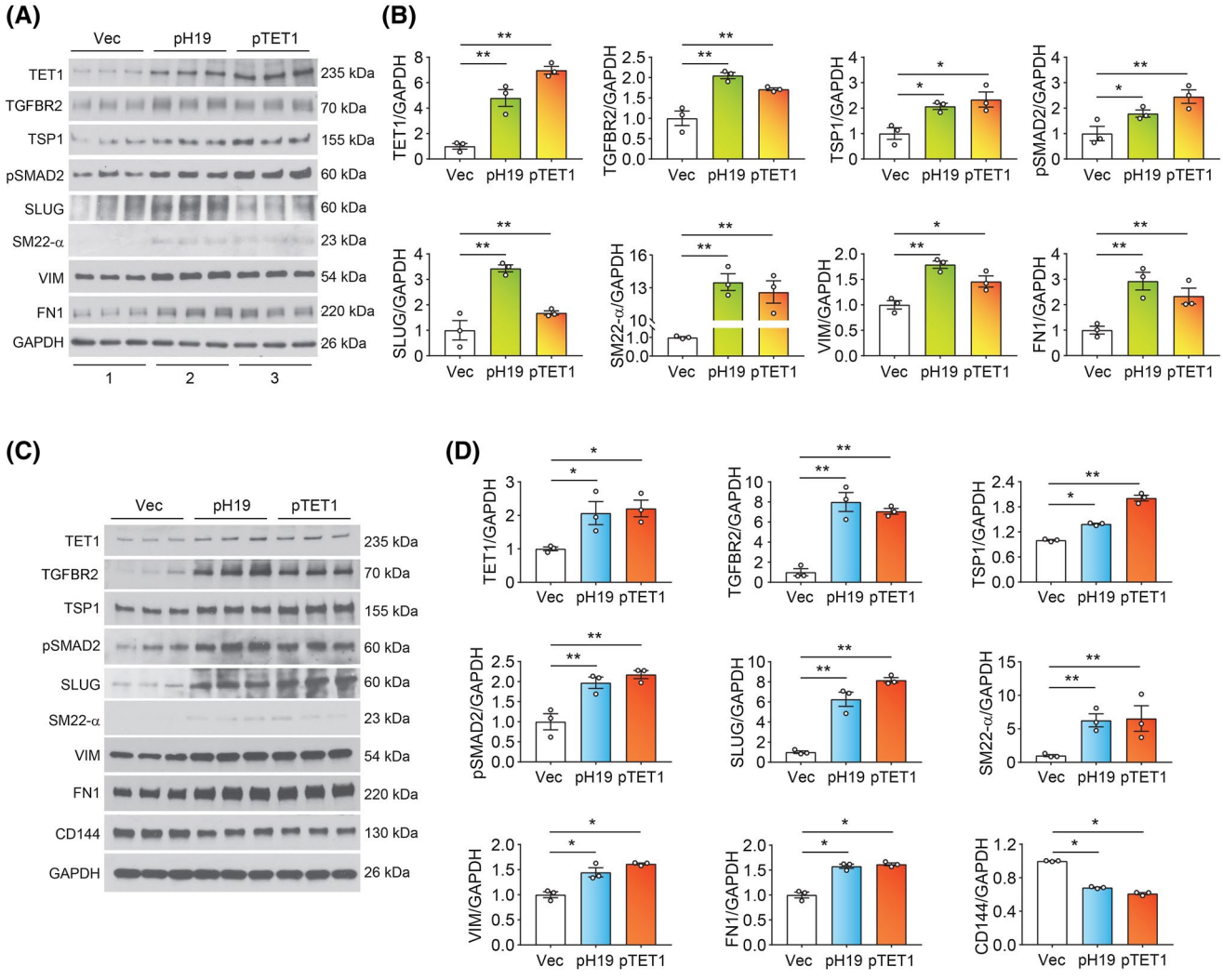

FIGURE 6 Overexpression of H19 or TET1 promotes TGF-β signaling and EndMT marker expression in vitro. HUVECs (A and B) or HAoECs (C and D) were transfected with empty vector, pH19, or pTET1. Proteins were extracted 48 hours post-transfection and analyzed by Western blot, with quantification of indicated proteins shown on the right. $*P < .05$; $**P < .01$. One-way ANOVA with Newman-Keuls post hoc test. Transfection experiments were carried out three times with one set of representative results shown. Error bars were calculated in technical replicate, n = 3

was accompanied by morphological changes of the cells (Figure S6). Together, these results suggest that H19 and TET1 promote TGF-β signaling contributing to EndMT in human primary ECs.

3.8 | H19 is required for upregulation of TGF-β signaling and EndMT in mouse ECs in vivo

To provide further evidence that the H19/TET1 axis regulates TGF-β β signaling and EndMT, we took advantage of a streptozotocin (STZ)-induced hyperglycemia mouse model. This model has been used by various groups to study vascular and pulmonary endothelial dysfunction, as hyperglycemia-induced oxidative stress promotes inflammation contributing to endothelial dysfunction.[58-60] An additional advantage of using this model is to provide relatively larger amounts of ECs (as opposed to isolation from segments of aortic tissues) for biochemical studies. Thus, wild-type (WT) and global H19 KO[61-63] mice were repeatedly injected with STZ (or vehicle as a control) to induce persistent hyperglycemia (a random plasma glucose level greater than 250 mg/dL that lasted for longer than 2 weeks). At 4 weeks after the initial injection, pulmonary microvascular ECs were isolated, followed by pathway gene expression analyses. There was a significant increase in circulating TNF-α levels in STZ- versus vehicle-treated animals in both WT and KO groups (Figure 7A), suggesting a hyperglycemia/oxidative stress-induced inflammatory milieu. Importantly, H19 expression in ECs from STZ-treated WT animals also increased (Figure 7B, compare white bar to green bar), consistent with glucose/TNF-α-stimulated upregulation of H19 observed in vitro (Figure 2A,B; Figure S3). In line with H19-mediated upregulation of TET1 and its downstream target genes, the expression of TET1, TGFBR2, and TSP1 increased in ECs of STZ-treated as compared to vehicle-treated WT animals (Figure 7C, top three blots, compare lane 2 to lane 1; Figure 7D, top three panels). This was accompanied by increased TGF-β signaling (as indicated by increased SMAD2 phosphorylation and SLUG expression) and increased EndMT marker expression (as indicated by increased expression of vimentin and fibronectin) (Figure 7B,C). In striking contrast, such changes in expression of TET1, TGF-β signaling genes, and EndMT markers were not observed between STZ- and vehicle-treated groups in the KO animals (Figure 7C,D). Although the animal numbers were limited (3-4 mice per group) and the experiments were exploratory in nature, the results further support the H19/TET1 axis as a novel and important regulator of endothelial TGF-β signaling and EndMT.

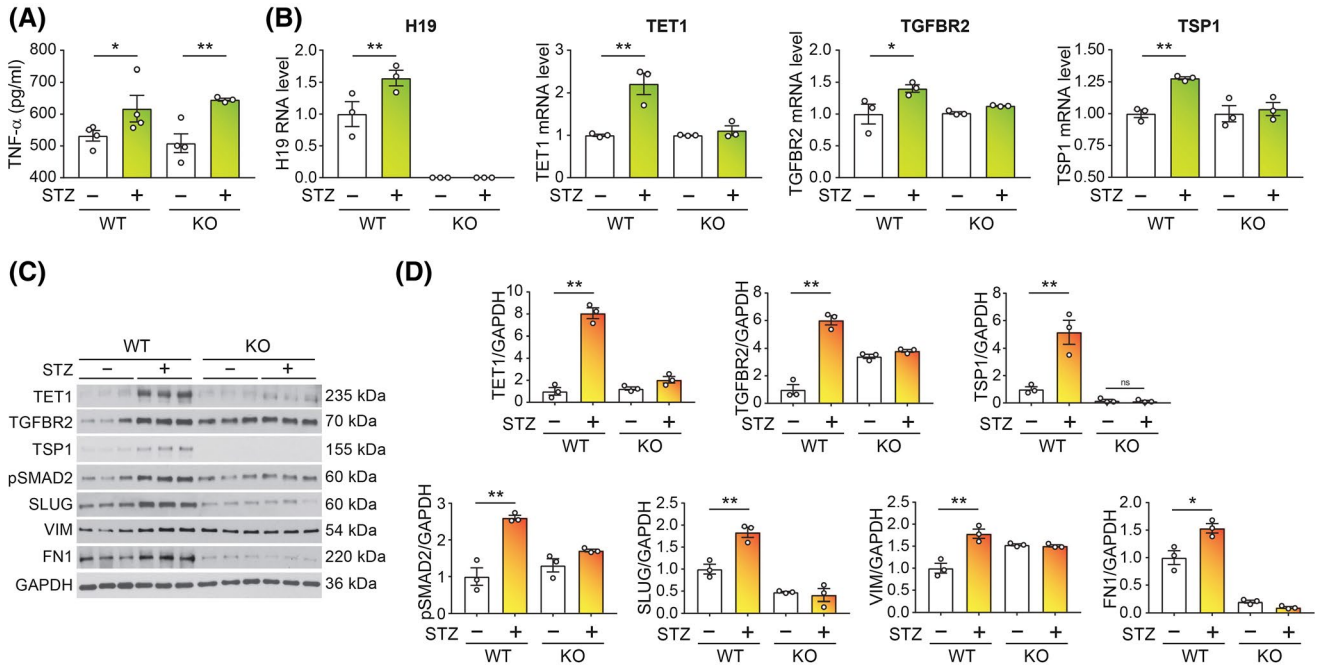

FIGURE 7 H19 depletion abrogates endothelial activation of TGF-β signaling and EndMT marker expression in vivo. A, ELISA analysis of serum TNF-α levels of WT and KO mice 2 weeks after initial injection of STZ (+) or vehicle (−), n =3- 4 animals per group. B, RT-qPCR analysis of expression of H19, TET1, TGFBR2, and TSP1 in lung ECs collected from WT and KO mice 5 weeks following initial injection of STZ (+) or vehicle (−). n = 3 animals per group. C, Western blot analysis of indicated proteins in lung ECs collected from WT and KO mice 5 weeks following initial injection of STZ (+) or vehicle (−). n = 3 animals per group. D, Quantification of proteins in C. *$P < .05$; **$P < .01$; ns, not statistically significant compared to control

4 | DISCUSSION

In this work, we describe the H19/TET1 axis as a novel regulator of TGF-β signaling and possibly EndMT in vascular ECs. Using multiple types of primary ECs from both human and mouse, we provide mechanistic evidence that inflammatory cytokine-induced upregulation of H19 promotes TET1 expression by reducing the bioavailability of let-7 and we identify TET1 as a new target of let-7-mediated regulation. We show that TET1 epigenetically regulates expression of TGFBR2 and TSP1, two key TGF-β signaling pathway genes, and that H19 and TET1 work in concert to stimulate TGF-β signaling and EndMT. Moreover, we demonstrate a striking correlation between increased endothelial expression of H19 and TET1, the extent of EndMT, and severity of atherosclerosis in human coronary arteries. Based on these results, we propose that endothelial activation of the H19/TET1 axis contributes to abnormal TGF-β signaling and EndMT. Our conclusion is further supported by a recent study showing that inhibiting H19 expression in aortic tissues in an ApoE KO atherosclerosis mouse model significantly attenuated disease progression.[9] Future studies using EC-specific H19 KO atherosclerosis animal models will be necessary to firmly establish an in vivo role of the H19/TET1 axis in EndMT.

We have previously documented that let-7 inhibits expression of TGFBR1 and that decreased endothelial FGFR1 signaling in response to soluble inflammatory stimuli reduces let-7 levels and increases TGFBR1 expression, leading to enhanced TGF-β signaling and EndMT.[24] In the present study, we show that let-7 inhibits TET1 expression and that TET1 promotes expression of TGFBR2 and TSP1 and TGF-β signaling. We also show that TNF-α upregulates endothelial expression of H19 reducing the bioavailability of let-7. It remains to be determined whether the FGFR1/TGFBR1 and H19/TET1 pathways operate in a synergistic way in ECs to promote TGF-β signaling and EndMT.

Decreased endothelial H19 expression was reported in human atherosclerotic plaques as compared to healthy arteries.[6] However, given that the H19 ISH and CD31 (endothelial marker) immunohistochemistry studies were performed separately on serial sections[6] (as opposed to H19 and CD31 co-staining on the same tissue sections), the possibility that a fraction of H19-positive cells might not be of endothelial origin could not be ruled out.

Enriched in mature vascular SMCs TET2 modulates SMC phenotype and plasticity.[11] TET2 was also shown to regulate autophagy in ECs.[12,13] We are the first to report that TET1 regulates TGF-β signaling and EndMT. While increased TET1 expression associates with atherosclerosis and severity of the disease (this report), decreased TET2 expression associates with atherosclerosis progression.[11-13] Future studies are warranted to determine whether the apparently opposite effects of TET1 and TET2 are due, in part, to cell type-specific functions (ie, ECs versus SMCs).

ECs from different blood vessels and different tissues have distinct and characteristic gene expression patterns. Our convergent results from human HUVECs (venous) and HAoECs (aortic) and mouse pulmonary microvascular ECs suggest that the H19/TET1-mediated pathway is likely conserved and active in various types of ECs, but not all. Indeed, a recent study of diabetic retinopathy showed decreased H19 expression in retinal ECs exposed to high glucose and H19 overexpression inhibited glucose-induced TGF-β1 upregulation and EndMT.[64] However, in these previous studies it was not clear how H19 upregulated TGF-β1 and whether an increase in TGF-β1 expression alone was sufficient to induce EndMT. Increased TGF-β1 expression does not always translate into increased TGF-β signaling which requires the coordinated actions of multiple factors including the ligands (ie, TGF-β1), the activators (ie, TSP1), and the receptors (ie, TGFBR2). Finally, as the retinal endothelium is part of the blood-retinal barrier comprising a single layer of non-fenestrated ECs with tight junctions,[65] the apparent discrepancy between findings from us and theirs[64] may reflect a district specificity.

In summary, we have identified a novel regulatory pathway mediated by the H19/TET1 axis in vascular ECs that is conserved between human and mouse and that functions to modulate TGF-β signaling and EndMT. This pathway may have a broad implication in various forms of CVD.

ACKNOWLEDGMENTS

We thank Dr Anjana Rao for the gift of plasmid FH-TET1-pEF. Research reported in this publication was supported by the National Institute of Diabetes and Digestive and Kidney Diseases of the National Institutes of Health under Award Number R01DK119386 to YH. The content is solely the responsibility of the authors and does not necessarily represent the official views of the National Institutes of Health. YH is the guarantor of this work and, as such, had full access to all the data in the study and takes responsibility for the integrity of the data and the accuracy of the data analysis.

CONFLICT OF INTEREST

All authors declare that they have no competing interests.

AUTHOR CONTRIBUTIONS

T. Cao, Y. Jiang, D. Li, L. Qin, G. Tellides, and Y. Huang designed research; T. Cao, Y. Jiang, D. Li, X. Sun, Y. Zhang, and L. Qin performed research; T. Cao, Y. Jiang, D. Li, and Y. Huang analyzed data; Y. Huang wrote the paper; H.S. Taylor provided intellectual insights and critical discussion of the project.

REFERENCES

1. Gao W, Zhu M, Wang H, et al. Association of polymorphisms in long non-coding RNA H19 with coronary artery disease risk in a Chinese population. *Mutat Res*. 2015;772:15-22.

2. Zhang Z, Gao W, Long QQ, et al. Increased plasma levels of lncRNA H19 and LIPCAR are associated with increased risk of coronary artery disease in a Chinese population. *Sci Rep*. 2017;7:7491.
3. Han DK, Khaing ZZ, Pollock RA, Haudenschild CC, Liau G. H19, a marker of developmental transition, is reexpressed in human atherosclerotic plaques and is regulated by the insulin family of growth factors in cultured rabbit smooth muscle cells. *J Clin Invest*. 1996;97:1276-1285.
4. Kim DK, Zhang L, Dzau VJ, Pratt RE. H19, a developmentally regulated gene, is reexpressed in rat vascular smooth muscle cells after injury. *J Clin Invest*. 1994;93:355-360.
5. Greco S, Zaccagnini G, Perfetti A, et al. Long noncoding RNA dysregulation in ischemic heart failure. *J Transl Med*. 2016;14:183.
6. Hofmann P, Sommer J, Theodorou K, et al. Long non-coding RNA H19 regulates endothelial cell aging via inhibition of STAT3 signalling. *Cardiovasc Res*. 2019;115:230-242.
7. Geng T, Liu Y, Xu Y, et al. H19 lncRNA promotes skeletal muscle insulin sensitivity in part by targeting AMPK. *Diabetes*. 2018;67:2183-2198.
8. Sun Y, Zhong L, He X, et al. LncRNA H19 promotes vascular inflammation and abdominal aortic aneurysm formation by functioning as a competing endogenous RNA. *J Mol Cell Cardiol*. 2019;131:66-81.
9. Yang Y, Tang F, Wei F, et al. Silencing of long non-coding RNA H19 downregulates CTCF to protect against atherosclerosis by upregulating PKD1 expression in ApoE knockout mice. *Aging*. 2019;11:10016-10030.
10. Wu X, Zhang Y. TET-mediated active DNA demethylation: mechanism, function and beyond. *Nat Rev Genet*. 2017;18:517-534.
11. Liu R, Jin Y, Tang WH, et al. Ten-eleven translocation-2 (TET2) is a master regulator of smooth muscle cell plasticity. *Circulation*. 2013;128:2047-2057.
12. Peng J, Yang Q, Li AF, et al. Tet methylcytosine dioxygenase 2 inhibits atherosclerosis via upregulation of autophagy in ApoE$^{-/-}$ mice. *Oncotarget*. 2016;7:76423-76436.
13. Yang Q, Li X, Li R, et al. Low shear stress inhibited endothelial cell autophagy through TET2 downregulation. *Ann Biomed Eng*. 2016;44:2218-2227.
14. Greissel A, Culmes M, Napieralski R, et al. Alternation of histone and DNA methylation in human atherosclerotic carotid plaques. *Thromb Haemost*. 2015;114:390-402.
15. Hong L, Du X, Li W, Mao Y, Sun L, Li X. EndMT: a promising and controversial field. *Eur J Cell Biol*. 2018;97:493-500.
16. Wesseling M, Sakkers TR, de Jager SCA, Pasterkamp G, Goumans MJ. The morphological and molecular mechanisms of epithelial/endothelial-to-mesenchymal transition and its involvement in atherosclerosis. *Vascul Pharmacol*. 2018;106:1-8.
17. Moonen JR, Lee ES, Schmidt M, et al. Endothelial-to-mesenchymal transition contributes to fibro-proliferative vascular disease and is modulated by fluid shear stress. *Cardiovasc Res*. 2015;108:377-386.
18. Chen PY, Qin L, Baeyens N, et al. Endothelial-to-mesenchymal transition drives atherosclerosis progression. *J Clin Invest*. 2015;125:4514-4528.
19. Evrard SM, Lecce L, Michelis KC, et al. Endothelial to mesenchymal transition is common in atherosclerotic lesions and is associated with plaque instability. *Nat Commun*. 2016;7:11853.
20. Aisagbonhi O, Rai M, Ryzhov S, Atria N, Feoktistov I, Hatzopoulos AK. Experimental myocardial infarction triggers canonical Wnt signaling and endothelial-to-mesenchymal transition. *Dis Model Mech*. 2011;4:469-483.
21. Maddaluno L, Rudini N, Cuttano R, et al. EndMT contributes to the onset and progression of cerebral cavernous malformations. *Nature*. 2013;498:492-496.
22. Piera-Velazquez S, Li Z, Jimenez SA. Role of endothelial-mesenchymal transition (EndoMT) in the pathogenesis of fibrotic disorders. *Am J Pathol*. 2011;179:1074-1080.
23. Kitao A, Sato Y, Sawada-Kitamura S, et al. Endothelial to mesenchymal transition via transforming growth factor-beta1/Smad activation is associated with portal venous stenosis in idiopathic portal hypertension. *Am J Pathol*. 2009;175:616-626.
24. Chen PY, Qin L, Barnes C, et al. FGF regulates TGF-beta signaling and endothelial-to-mesenchymal transition via control of let-7 miRNA expression. *Cell Rep*. 2012;2:1684-1696.
25. Cooley BC, Nevado J, Mellad J, et al. TGF-beta signaling mediates endothelial-to-mesenchymal transition (EndMT) during vein graft remodeling. *Sci Transl Med*. 2014;6:227ra234.
26. Zeisberg EM, Tarnavski O, Zeisberg M, et al. Endothelial-to-mesenchymal transition contributes to cardiac fibrosis. *Nat Med*. 2007;13:952-961.
27. Jeong D, Lee MA, Li Y, et al. Matricellular protein CCN5 reverses established cardiac fibrosis. *J Am Coll Cardiol*. 2016;67:1556-1568.
28. Li DY, Busch A, Jin H, et al. H19 induces abdominal aortic aneurysm development and progression. *Circulation*. 2018;138:1551-1568.
29. Jimenez SA, Piera-Velazquez S. Endothelial to mesenchymal transition (EndoMT) in the pathogenesis of systemic sclerosis-associated pulmonary fibrosis and pulmonary arterial hypertension. Myth or reality? *Matrix Biol*. 2016;51:26-36.
30. Murphy-Ullrich JE, Suto MJ. Thrombospondin-1 regulation of latent TGF-beta activation: a therapeutic target for fibrotic disease. *Matrix Biol*. 2018;68-69:28-43.
31. Meng XM, Nikolic-Paterson DJ, Lan HY. TGF-beta: the master regulator of fibrosis. *Nat Rev Nephrol*. 2016;12:325-338.
32. DiPietro LA, Nebgen DR, Polverini PJ. Downregulation of endothelial cell thrombospondin 1 enhances in vitro angiogenesis. *J Vasc Res*. 1994;31:178-185.
33. Reed MJ, Iruela-Arispe L, O'Brien ER, et al. Expression of thrombospondins by endothelial cells. Injury is correlated with TSP-1. *Am J Pathol*. 1995;147:1068-1080.
34. Kessler T, Zhang L, Liu Z, et al. ADAMTS-7 inhibits re-endothelialization of injured arteries and promotes vascular remodeling through cleavage of thrombospondin-1. *Circulation*. 2015;131:1191-1201.
35. Chen D, Asahara T, Krasinski K, et al. Antibody blockade of thrombospondin accelerates reendothelialization and reduces neointima formation in balloon-injured rat carotid artery. *Circulation*. 1999;100:849-854.
36. Moura R, Tjwa M, Vandervoort P, Cludts K, Hoylaerts MF. Thrombospondin-1 activates medial smooth muscle cells and triggers neointima formation upon mouse carotid artery ligation. *Arterioscler Thromb Vasc Biol*. 2007;27:2163-2169.
37. Kallen AN, Zhou XB, Xu J, et al. The imprinted H19 lncRNA antagonizes let-7 microRNAs. *Mol Cell*. 2013;52:101-112.
38. Tahiliani M, Koh KP, Shen Y, et al. Conversion of 5-methylcytosine to 5-hydroxymethylcytosine in mammalian DNA by MLL partner TET1. *Science*. 2009;324:930-935.
39. Akazawa Y, Cazanave S, Mott JL, et al. Palmitoleate attenuates palmitate-induced Bim and PUMA up-regulation and hepatocyte lipoapoptosis. *J Hepatol*. 2010;52:586-593.
40. Lanahan AA, Hermans K, Claes F, et al. VEGF receptor 2 endocytic trafficking regulates arterial morphogenesis. *Dev Cell*. 2010;18:713-724.

41. Iwasaki S, Kawamata T, Tomari Y. *Drosophila* argonaute1 and argonaute2 employ distinct mechanisms for translational repression. *Mol Cell*. 2009;34:58-67.
42. Zhang Z, Weaver DL, Olsen D, et al. Long non-coding RNA chromogenic in situ hybridisation signal pattern correlation with breast tumour pathology. *J Clin Pathol*. 2016;69:76-81.
43. Jiang Y, Huang Y, Cai S, et al. H19 is expressed in hybrid hepatocyte nuclear factor 4alpha(+) periportal hepatocytes but not cytokeratin 19(+) cholangiocytes in cholestatic livers. *Hepatol Commun*. 2018;2:1356-1368.
44. Kruger J, Rehmsmeier M. RNAhybrid: microRNA target prediction easy, fast and flexible. *Nucleic Acids Res*. 2006;34:W451-W454.
45. Khambhati J, Engels M, Allard-Ratick M, Sandesara PB, Quyyumi AA, Sperling L. Immunotherapy for the prevention of atherosclerotic cardiovascular disease: promise and possibilities. *Atherosclerosis*. 2018;276:1-9.
46. Clarke R, Daly L, Robinson K, et al. Hyperhomocysteinemia: an independent risk factor for vascular disease. *N Engl J Med*. 1991;324:1149-1155.
47. Li T, Yu B, Liu Z, et al. Homocysteine directly interacts and activates the angiotensin II type I receptor to aggravate vascular injury. *Nat Commun*. 2018;9:11.
48. Ghazal S, McKinnon B, Zhou J, et al. H19 lncRNA alters stromal cell growth via IGF signaling in the endometrium of women with endometriosis. *EMBO Mol Med*. 2015;7:996-1003.
49. Gao Y, Wu F, Zhou J, et al. The H19/let-7 double-negative feedback loop contributes to glucose metabolism in muscle cells. *Nucleic Acids Res*. 2014;42:13799-13811.
50. Zuckerwise L, Li J, Lu L, et al. H19 long noncoding RNA alters trophoblast cell migration and invasion by regulating TbetaR3 in placentae with fetal growth restriction. *Oncotarget*. 2016;7:38398-38407.
51. Fabian MR, Sonenberg N. The mechanics of miRNA-mediated gene silencing: a look under the hood of miRISC. *Nat Struct Mol Biol*. 2012;19:586-593.
52. Yan L, Zhou J, Gao Y, et al. Regulation of tumor cell migration and invasion by the H19/let-7 axis is antagonized by metformin-induced DNA methylation. *Oncogene*. 2015;34:3076-3084.
53. Yamashita S, Takahashi S, McDonell N, et al. Methylation silencing of transforming growth factor-beta receptor type II in rat prostate cancers. *Cancer Res*. 2008;68:2112-2121.
54. Stenina-Adognravi O. Invoking the power of thrombospondins: regulation of thrombospondins expression. *Matrix Biol*. 2014;37:69-82.
55. Cao T, Jiang Y, Wang Z, et al. H19 lncRNA identified as a master regulator of genes that drive uterine leiomyomas. *Oncogene*. 2019;38:5356–5366.
56. Zhou J, Yang L, Zhong T, et al. H19 lncRNA alters DNA methylation genome wide by regulating S-adenosylhomocysteine hydrolase. *Nat Commun*. 2015;6:10221.
57. Zhong T, Men Y, Lu L, et al. Metformin alters DNA methylation genome-wide via the H19/SAHH axis. *Oncogene*. 2017;36:2345-2354.
58. Popov D, Simionescu M. Structural and transport property alterations of the lung capillary endothelium in diabetes. *Ital J Anat Embryol*. 2001;106:405-412.
59. Uyy E, Antohe F, Ivan L, Haraba R, Radu DL, Simionescu M. Upregulation of caveolin-1 expression is associated with structural modifications of endothelial cells in diabetic lung. *Microvasc Res*. 2010;79:154-159.
60. Li P, Yin YL, Guo T, et al. Inhibition of aberrant microRNA-133a expression in endothelial cells by statin prevents endothelial dysfunction by targeting GTP cyclohydrolase 1 in vivo. *Circulation*. 2016;134:1752-1765.
61. Ripoche MA, Kress C, Poirier F, Dandolo L. Deletion of the H19 transcription unit reveals the existence of a putative imprinting control element. *Genes Dev*. 1997;11:1596-1604.
62. Martinet C, Monnier P, Louault Y, Benard M, Gabory A, Dandolo L. H19 controls reactivation of the imprinted gene network during muscle regeneration. *Development*. 2016;143:962-971.
63. Zhang N, Geng T, Wang Z, et al. Elevated hepatic expression of H19 long noncoding RNA contributes to diabetic hyperglycemia. *JCI Insight*. 2018;3:e120304.
64. Thomas AA, Biswas S, Feng B, Chen S, Gonder J, Chakrabarti S. lncRNA H19 prevents endothelial-mesenchymal transition in diabetic retinopathy. *Diabetologia*. 2019;62:517-530.
65. El-Remessy AB, Al-Shabrawey M, Khalifa Y, Tsai NT, Caldwell RB, Liou GI. Neuroprotective and blood-retinal barrier-preserving effects of cannabidiol in experimental diabetes. *Am J Pathol*. 2006;168:235-244.

SUPPORTING INFORMATION

Additional Supporting Information may be found online in the Supporting Information section.

How to cite this article: Cao T, Jiang Y, Li D, et al. H19/TET1 axis promotes TGF-β signaling linked to endothelial-to-mesenchymal transition. *The FASEB Journal*. 2020;34:8625–8640. https://doi.org/10.1096/fj.202000073RRRRR